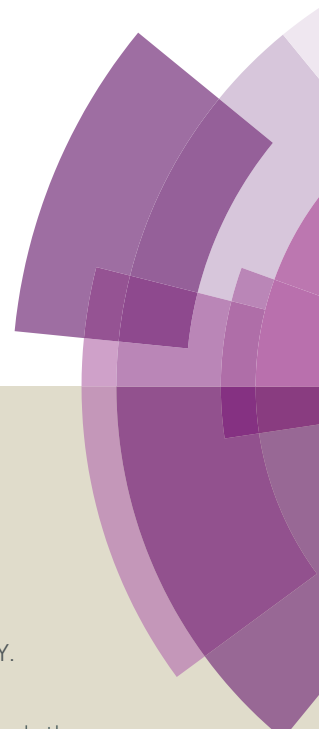


Journal of Materials Chemistry A

Accepted Manuscript



This article can be cited before page numbers have been issued, to do this please use: Y. Wu, C. Cao, Y. Zhu, J. Li and L. Wang, *J. Mater. Chem. A*, 2015, DOI: 10.1039/C5TA03225C.



This is an *Accepted Manuscript*, which has been through the Royal Society of Chemistry peer review process and has been accepted for publication.

Accepted Manuscripts are published online shortly after acceptance, before technical editing, formatting and proof reading. Using this free service, authors can make their results available to the community, in citable form, before we publish the edited article. We will replace this *Accepted Manuscript* with the edited and formatted *Advance Article* as soon as it is available.

You can find more information about *Accepted Manuscripts* in the [Information for Authors](#).

Please note that technical editing may introduce minor changes to the text and/or graphics, which may alter content. The journal's standard [Terms & Conditions](#) and the [Ethical guidelines](#) still apply. In no event shall the Royal Society of Chemistry be held responsible for any errors or omissions in this *Accepted Manuscript* or any consequences arising from the use of any information it contains.

ARTICLE

Cube-shaped hierarchical $\text{LiNi}_{1/3}\text{Co}_{1/3}\text{Mn}_{1/3}\text{O}_2$ with enhanced growth of nanocrystal planes as high-performance cathode materials for lithium-ion batteries

Cite this: DOI: 10.1039/x0xx00000x

Received 00th January 2012,
Accepted 00th January 2012

DOI: 10.1039/x0xx00000x

www.rsc.org/Yu Wu,^a Chuanbao Cao,*^a Youqi Zhu,^a Jili Li^b and Lin Wang^a

Hierarchical cubed $\text{LiNi}_{1/3}\text{Co}_{1/3}\text{Mn}_{1/3}\text{O}_2$ with enhanced growth of electrochemically active planes (CH-NCM) are synthesized using cube structured MnCO_3 as a self-template, which is synthesized by a fast, simple, and surfactant-free co-precipitation method. The CH-NCM cathode has a reversible discharge capacity as high as 220.9, 216.2, 211.4, 189.6, 171.7 and 144.5 mA h g^{-1} at 0.1, 0.5, 1, 2, 5, and 10 C, respectively. After 100 cycles, the capacity retention is 83.34% at 0.1 C. The superior electrochemical performance can be ascribed to the special cube-shaped hierarchical structure and enhanced growth of electrochemically active surface planes of the CH-NCM. The primary nanoparticles with enhanced growth of electrochemically active surface planes, guarantee ultrafast Li^+ intercalation/deintercalation, while the submicroassemblies promise the good structural stability.

Introduction

Lithium-ion batteries have played an important role in portable electronics, and are intensively pursued as a power source for vehicle applications.^{1,2} LiCoO_2 was the first cathode material used in commercial Lithium-ion batteries,³ but its limited capacity, high cost and toxicity prohibit its use in vehicle applications. To overcome the current drawbacks, layered $\text{LiNi}_{1/3}\text{Co}_{1/3}\text{Mn}_{1/3}\text{O}_2$ (NCM) has been widely investigated by many researchers due to its advantages of highly reversible capacity, low safety hazard and relatively low cost.⁴⁻¹⁹ However, layered $\text{LiNi}_{1/3}\text{Co}_{1/3}\text{Mn}_{1/3}\text{O}_2$ exhibits rapid fading capacity and inferior rate capability, which prevent its use in vehicle applications.

Recently, hierarchical micro-/nanostructures have attracted considerable interests because the nanometer-sized primary particles can signally shorten the pathways for lithium ion and electron, and the micro-/submicrometer-sized secondary assemblies can ensure the easy manufacture and good stability.^{5,20,21} Hierarchical electrode materials with high reversible capacity and improved cyclability have been widely reported²²⁻²⁶. NCM with a hexagonal layer $\alpha\text{-NaFeO}_2$ structure, which is made up of MO_2 oxygen layers perpendicular to the c axis,⁸ indexed as {001} planes that include the (00 $\bar{1}$) and (001) planes at the top and bottom, respectively of the hexagonal crystal. The {001} planes are formed by NiO_6 , CoO_6 and MnO_6 octahedra, which interconnect to each other by corner-sharing oxygen atoms, and consist of a close-packed structure that hinders Li^+ insertion along the c axis. The close packed {001} planes are therefore not electrochemically active for Li^+ transportation. The 6-sided facets of the hexagonal crystal, i.e. (010), (0 $\bar{1}$ 0), (100), (110), (1 $\bar{1}$ 0) and (1 $\bar{0}$ 0) planes, are denoted as {010} planes, which are perpendicular to the {001} planes

and have an open structure with a wide window between the layers for Li^+ transportation.¹¹ This structural analysis indicates that Li^+ transport in NCM is two-dimensional parallel to the Li^+ layers along the a (or b) axis. Therefore, if most nanocrystal planes are parallel to (010), (110), and (100) planes, perpendicular to (001) plane, the rate performance of NCM will be significantly improved. In our previous reported works, NCM nanoplates with exposed {010} active planes have been proved to exhibit superior rate performance.¹¹ Hence, the hierarchical NCM with enhanced growth of electrochemically active planes can be expected to achieve enhanced comprehensive electrochemical performance. Unfortunately, the {010} active planes have higher surface energy than {001} planes through calculation. Because the high surface energy planes grow faster than the low surface energy planes, the high surface energy planes tend to vanish during growth. Up to now, it remains a big challenge to synthesize hierarchical NCM materials with enhanced growth of electrochemically active planes.

Although the literature has reported how to synthesize cube structured materials,²⁷⁻³¹ most of synthesis technologies are sophisticated, time-consuming. In this work, we report a convenient co-precipitation method, coupled with heat treatment, to synthesize cube-shaped hierarchical $\text{LiNi}_{1/3}\text{Co}_{1/3}\text{Mn}_{1/3}\text{O}_2$ (CH-NCM) materials with enhanced growth of electrochemically active planes {010} for the first time. This co-precipitation method is fast, simple, and surfactant-free chemical route, in which MnCO_3 cubes as both a self-template and Mn source was firstly formed and then lithiation reaction was done to develop the CH-NCM at high temperature. The CH-NCM are about 400-600 nm in size, and consist of aggregates of approximately 100 nm primary nanoparticles. The CH-NCM cathode has a reversible discharge capacity as high as 220.9 mA h g^{-1} , 216.2 mA h g^{-1} , 211.4 mA h g^{-1} , 189.6 mA h g^{-1} , 171.7 mA h g^{-1} , and 144.5

ARTICLE

ma h g⁻¹ at 0.1 C, 0.5 C, 1 C, 2 C, 5 C, and 10 C rates, respectively. What is more, the capacity retention is also significantly improved. After 100 charge-discharge cycles, capacity retention ratios are 83.34% (0.1 C), 79.33% (1 C), and 73.36% (2 C), respectively.

Experimental

Preparation of CH-NCM

Firstly, MnCO₃ cubes with sizes of about 400-600 nm were obtained by the method reported in the previous literature with minor modifications.³² Typically, 1 mmol MnSO₄ was dissolved in 70 mL deionized water at room temperature. Then 350 mL ethanol was added to the MnSO₄ solution under stirring, after its complete dispersion, a solution of 10 mmol NH₄HCO₃ dissolved in 70 mL deionized water was added to the solution mentioned above. After vigorous stirring for 15 min, the MnCO₃ cubes were separated by centrifugation, and washed with deionized water and ethanol to remove impurities. Then, the MnCO₃ cubes were dried and decomposed at 400 °C to obtain MnO₂ cubes. After that, the MnO₂ cubes were dispersed along with stoichiometric amounts of Ni(NO₃)₂·6H₂O, Co(NO₃)₂·6H₂O and LiOH·H₂O in ethanol to form suspension. The suspension was then evaporated at room temperature until dryness. Finally, the mixture was ground manually for 10 min, heated at 850 °C for 12 h in air.

Characterization

The crystal structures of the prepared products were analyzed using a PANalytical X-pert diffractometer (PANalytical, Netherlands) with Cu K α radiation. X-ray photoelectron spectroscopy (XPS) (PHI Quanteral II, Japan) were conducted to evaluate the oxidation states of the Ni, Co and Mn in the prepared samples and the fittings were carried out by the XPSPEAK41 program. The chemical compositions of the samples were analyzed by inductively coupled plasma atomic emission spectrometry (ICP-AES, ICAP-6300). Hitachi field-emission scanning electron microscopy (FESEM, Hitachi S-4800) was used to analyze the structure and morphology of the samples. Transmission electron microscopy (TEM) (HRTEM, FEI Tecnai G2 F20, 200 kV) was used to observe the crystal structure of the samples.

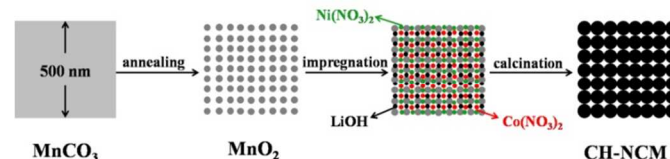
Electrochemical measurements

Electrochemical measurements were carried out in CR2025 coin-type cells which were assembled in an Ar-filled glove box using Celgard 2400 films as the separator, a solution of 1 M LiPF₆ dissolved into ethyl carbonate–dimethyl carbonate (EC–DMC, 1 : 1 v/v) as electrolyte, and lithium foil as the counter and reference electrodes. The cathode electrodes were prepared by mixing 80 wt% sample, 10 wt% carbon black, and 10 wt% polyvinylidene fluoride (PVDF) binder, dissolved in N-methyl-2-pyrrolidone (NMP) to form a slurry. The slurry was coated on Al foil and dried at 120 °C in vacuum for 12 hours. Charge–discharge tests were performed at different current rates between 2.5 and 4.5 V on a CT2001A Land battery testing system. Cyclic voltammetry (CV; 2.5–4.5 V, 0.1 mV s⁻¹) and electrochemical impedance spectroscopic (EIS) measurements were conducted on an IM6e electrochemical workstation (Zahner, Germany). EIS measurements were carried out with a frequency range of 100 kHz to 0.1 Hz and an AC voltage of 5 mV. All tests were performed at room temperature.

Results and discussion

Scheme 1 illustrates the formation process of the CH-NCM. MnCO₃

cubes (Fig. S1) prepared by the co-precipitation method are employed as a self-template and Mn source in the synthesis. Firstly, MnCO₃ cubes are converted into MnO₂ cubes (Fig. S2) by thermal decomposition at 400 °C. Then, the cube-shaped MnO₂ are mixed along with stoichiometric amounts of Ni(NO₃)₂·6H₂O, Co(NO₃)₂·6H₂O and LiOH·H₂O. Lastly, the calcinations process is necessary to form the CH-NCM.



Scheme 1 The preparation of CH-NCM

The XRD patterns of CH-NCM are shown in Fig. 1. The sharp reflections in the XRD patterns reveal that the as-prepared materials are well-crystallized. All of the peaks can be indexed as a hexagonal α -NaFeO₂ structure with a R $\bar{3}$ m space group, indicating that the CH-NCM without an impure phase.^{17,33} The clear separations of the (006) from the (102) and the (108) from the (110) peaks suggest the formation of a well-ordered hexagonal layered structure. For the XRD patterns of CH-NCM, the intensity ratio of the (003) and (104) peaks ($I_{(003)}/I_{(104)}$) is 1.43, which is larger than 1.2 indicating low cation mixing.^{5,33}

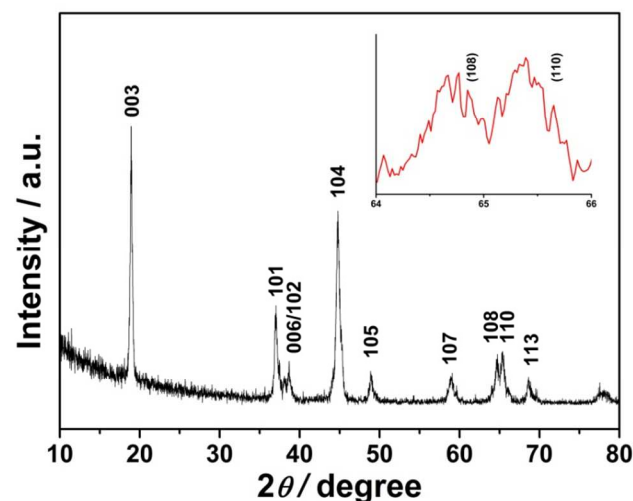


Fig. 1 XRD patterns of CH-NCM.

X-ray photoelectron spectroscopy (XPS) measurements were carried out to confirm the oxidation states of Ni, Co and Mn in CH-NCM. Assisted by a fitting process, the assignment of the main peak and the satellite is well established. As shown in Fig. 2, the binding energies of Ni2p_{3/2}, Co2p_{3/2} and Mn2p_{3/2} are 853.65 eV, 779.02 eV and 641.25 eV, respectively. These values agree well with the oxidation states of Ni²⁺, Co³⁺ and Mn⁴⁺.³⁴ The exact ratios of Li: Ni: Co: Mn measured by ICP-AES is 3.00: 0.97: 1.09: 0.96 for CH-NCM, which is the same as the designed value.

The morphology and structure of the MnO₂ precursors and the CH-NCM were characterized by FE-SEM and TEM. Fig. 3A and B show the FE-SEM images of the MnO₂ precursors at low and high magnifications, respectively. It is clearly found that the MnO₂ precursors show relatively uniform sizes of about 400-600 nm with a

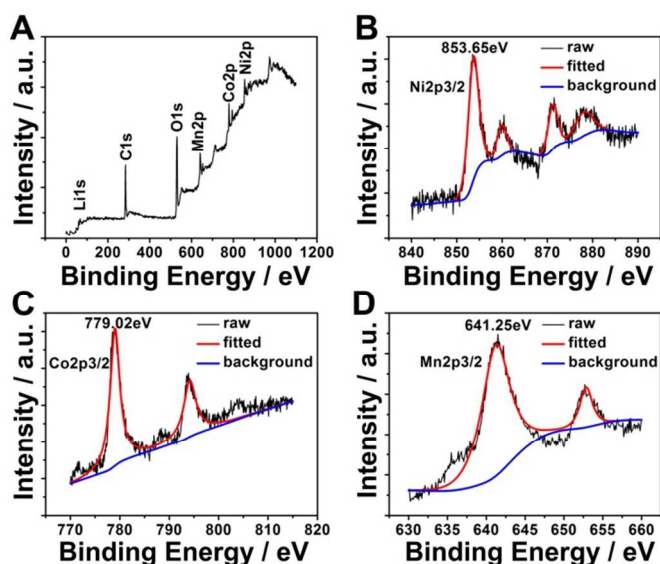


Fig. 2 (A) XPS curves of CH-NCM; (B), (C), and (D) XPS curves of the Ni 2p, Co 2p, and Mn 2p core level for CH-NCM.

cube-like morphology. From the high magnifications FE-SEM image of the MnO_2 precursors, we can distinctly observe the edges and faces of the cube. Fig. 3C shows a FE-SEM image of the CH-NCM. It is obvious that the cube-shaped hierarchical architectures are maintained after the high temperature solid state reaction. Compared with the cube-shaped MnO_2 precursors, the faces of CH-NCM are rough due to the crystal growth in the high temperature sintering process. To further prove the cube-shaped hierarchical structure, magnified FE-SEM images and TEM image of the CH-NCM are shown in Fig. 3D and Fig. S3, revealing CH-NCM with aggregates of approximately 100 nm primary nanoparticles.

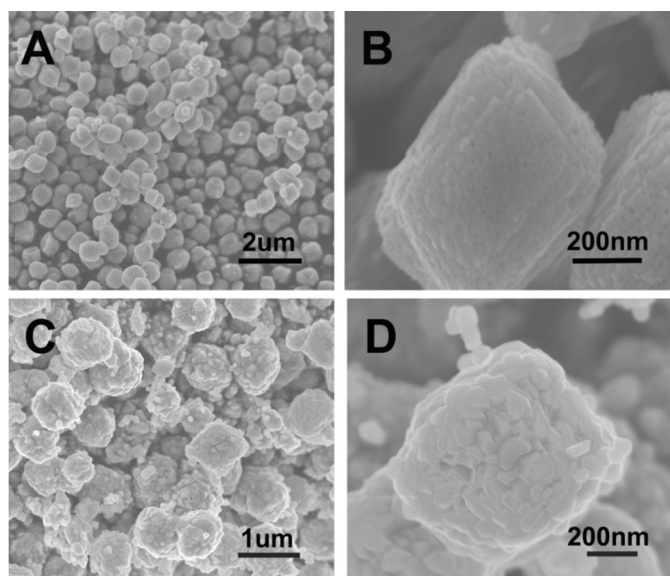


Fig. 3 (A) and (B) FE-SEM images at different magnifications of the MnO_2 precursors; (C) and (D) FE-SEM images at different magnifications of CH-NCM.

Fig. 4A and C show the TEM images of CH-NCM. The cube-shaped hierarchical structure can be observed clearly, which is consistent with the above FE-SEM images. Fig. 4B depicts lattice fringes of the plane with spacing of 0.475 nm shown in Fig. 4A,

corresponding to the (003) planes of the NCM cathode materials. This implies that the projected image planes of the primary nanoplates are parallel to the c-axis direction (parallel to (100), (010), or (110) planes).²⁶ Such characteristic lattice spacing can be frequently observed in the investigation of primary nanoplates of the CH-NCM material (Fig. S4). Fig. 4D shows the HR-TEM image of the plane in Fig. 4C and its corresponding Fast Fourier Transform (FFT) pattern (the inset image). There are three sets of clear fringes. Two of them have the same interplanar distance of 0.246 nm assigned to the (0 $\bar{1}$ 0) and (100) planes of NCM, respectively. And the other one has an interplanar distance of 0.143 nm assigned to (110) planes of NCM. The FFT pattern reveals these nanoplates are single crystalline with a hexagonal symmetry in consistency with the hexagonal structure of NCM. As what mentioned before, Li^+ preferably moves two-dimensionally along the a-b planes ((001) plane) in hexagonal layer NCM materials. Therefore, we can conclude that the enhanced growth of electrochemically active planes in favor of Li^+ intercalation/deintercalation has been successfully achieved for the CH-NCM cathode material.

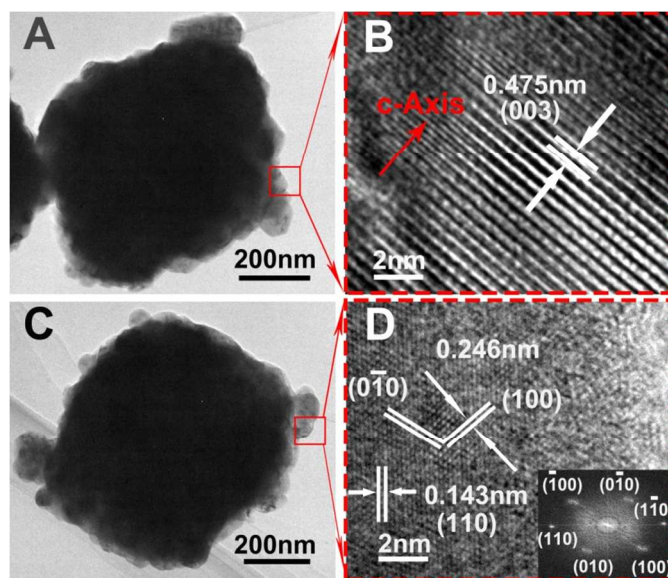


Fig. 4 (A) TEM image of the CH-NCM. (B) HRTEM image of the plane shown in (A). (C) TEM image of the CH-NCM. (D) HRTEM image and fast Fourier transform (FFT) pattern of plane shown in (C).

To evaluate the electrochemical properties of the CH-NCM as cathode materials for lithium-ion batteries, standard CR2025 coin-type half cells are assembled in an Ar-filled glove box. Fig. 5A shows the cycle performances of the as-prepared materials at various current rates. The initial discharge capacities are 220.9 mA h g^{-1} , 211.4 mA h g^{-1} , and 189.6 mA h g^{-1} at 0.1 C, 1 C, and 2 C rates, respectively. After 100 cycles, the discharge capacities of CH-NCM are maintained at 184.1 mA h g^{-1} (0.1 C), 167.7 mA h g^{-1} (1 C), and 139.1 mA h g^{-1} (2 C), with the capacity retention ratios are 83.34% (0.1 C), 79.33% (1 C), and 73.36% (2 C), respectively. Comparative cycling performances of CH-NCM and NCM-bulk at 2 C as shown in Fig. S5. The initial discharge capacity of NCM-bulk is far less than that of CH-NCM. After 100 charge-discharge cycles, the CH-NCM exhibits better cycle life (73.36% of capacity retention) than NCM-bulk cathodes (57.75% of capacity retention). Fig. 5B shows the coulombic efficiencies of CH-NCM at current rate of 0.1 C and 1 C, respectively. The average coulombic efficiencies are 98.98% (0.1 C) and 98.49% (1 C), which indicated that the cell exhibited high reversible capacity. Besides the high specific capacity and good

cycle performance, the rate capability is also a very important property for cathode materials. To evaluate the rate capability, the CH-NCM was cycled at various charge/discharge rates from 0.5 to 10 C during 2.5–4.5 V with 5 cycles per step. When the charge/discharge rates were higher than 1 C, a constant voltage

capacity was still maintained at 144.5 mA h g⁻¹ even at the highest rate of 10 C. Significantly, the discharge capacity can be recovered to nearly its primal value when cycling back to 0.5 C rate. These results indicated that this material has a superior rate capability.

Fig. 6A and B show the galvanostatic charge-discharge profiles of CH-NCM in the 1st, 2nd, 10th, 30th, 50th, and 100th cycles at current rate of 0.1 C and 1 C, respectively. Surprisingly, the smooth charge and discharge profiles with little voltage drop can be clearly observed, indicating that the steady CH-NCM electrode structural integrity in the test voltage range.^{5,35} The irreversible capacity loss of CH-NCM during the first cycle may be attributed to the formation of a solid electrolyte interlayer.³³ Compared to other NCM cathode materials,^{5,6,9-14} the CH-NCM has superior electrochemical performances, especially in terms of rate capability (Table S1). We believe that the obvious improvement of the rate capability mainly be ascribed to the special hierarchical structured cubes and enhanced growth of electrochemically active surface planes of the CH-NCM. The primary nanoparticles with enhanced growth of electrochemically active surface planes, guarantee ultrafast Li⁺ intercalation/deintercalation as well as Li⁺ diffusion, while the submicroassemblies promise the good structural stability. The morphologies of the CH-NCM after 100 charge-discharge cycles are shown in Fig. S6, which suggest that the CH-NCM cathodes can maintain their initial morphology at 0.1 C. Besides, electrochemical inactivity of

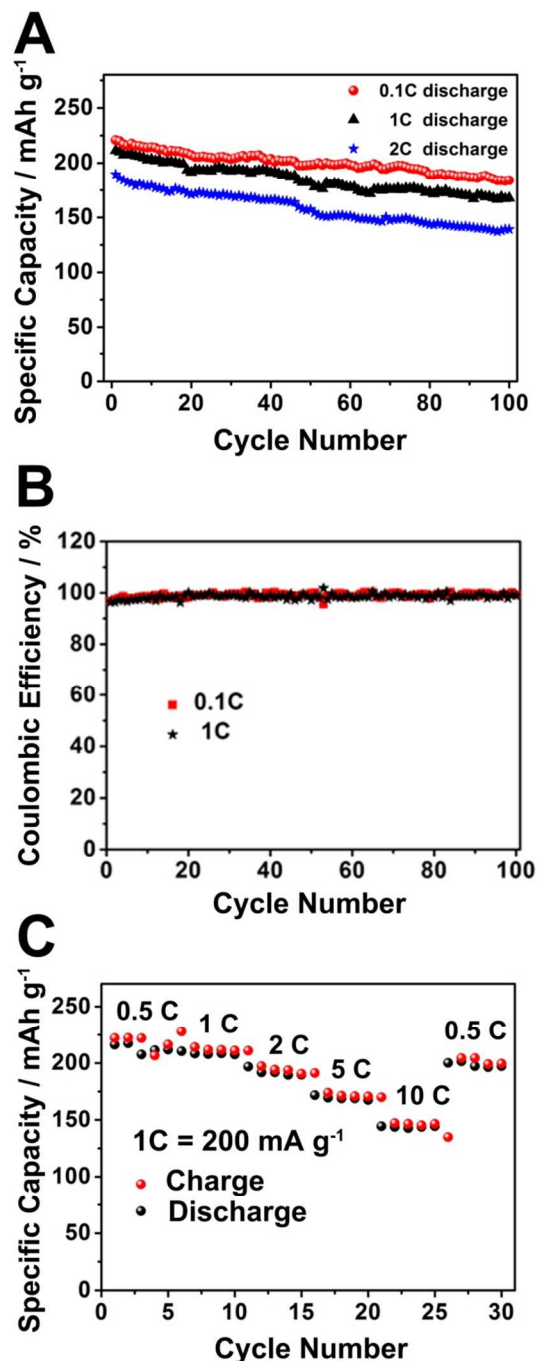


Fig. 5 (A) Comparative cycling performances of CH-NCM at various current rates; (B) Coulombic efficiencies of CH-NCM at current rate of 0.1 C and 1 C, respectively; (C) Rate capability of CH-NCM.

charge step was used for 30 minutes after the constant current charge step to reach the predetermined voltage.¹¹ Fig. 5C shows the rate capability of as-prepared materials. A initial discharge capacities of 216.2 mA h g⁻¹ and 171.7 mA h g⁻¹ were obtained at 0.5 C and 5 C, respectively. What is more, it is clearly found that the discharge

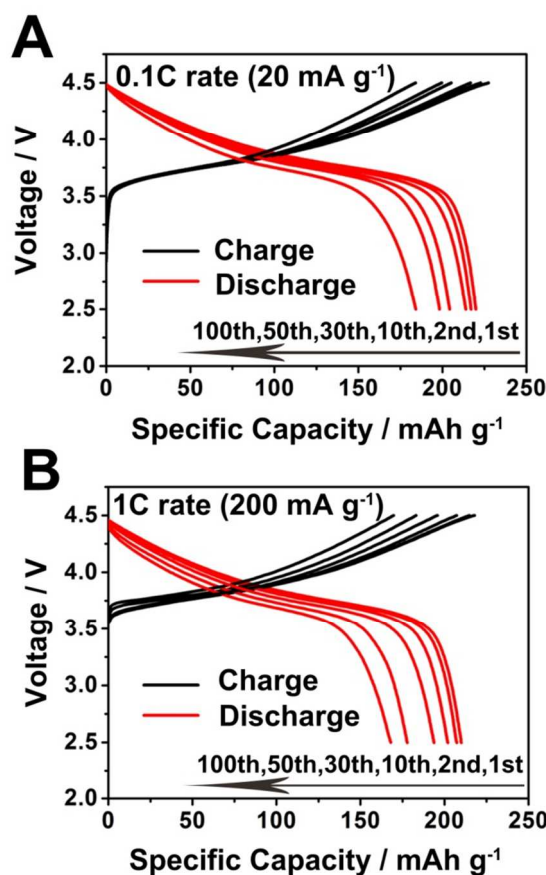


Fig. 6 (A) and (B) Galvanostatic charge-discharge profiles of CH-NCM in the 1st, 2nd, 10th, 30th, 50th, and 100th cycles at current rate of 0.1 C and 1 C, respectively.

tetravalent Mn ions in $\text{LiNi}_{1/3}\text{Co}_{1/3}\text{Mn}_{1/3}\text{O}_2$ can effectively prevent capacity fading caused by Mn element dissolution and Jahn-Teller distortion.⁹

The charge-transfer kinetics was investigated by CV and EIS as shown in Fig. 7. Among the three transition-metal elements of CH-NCM, Ni and Co with main oxidation states +2 and +3, respectively, are known to be electrochemically active and Mn with +4 oxidation state is not active. The first three representative CV curves of CH-NCM between 2.5 and 4.5 V are shown in Fig. 7A. The CV curves exhibit an oxidation peak at 3.97 V and a corresponding reduction peak at 3.66 V, which corresponds to redox transition of $\text{Ni}^{2+}/\text{Ni}^{4+}$. No obvious Co transition redox peaks are observed because $\text{Co}^{3+}/\text{Co}^{4+}$ conversion comes up at a potential higher than 4.6 V.³⁶ With the increased cycles, the oxidation peak decreased from 3.97 V to the lower value and stabilized at 3.93 V; this behavior also indicated that the material structure and/or the electrode – electrolyte interface were modified after the initial cycles.^{37,38} Fig. 7B shows the EIS profiles of the CH-NCM electrode after different charge-discharge cycles. As it was described in the previous work,⁵ a high-frequency semicircle, an intermediate-frequency semicircle and a low-frequency oblique line are observed. The high-frequency semicircle ascribes to the solid electrolyte interface (SEI) resistance (RSEI). The intermediate-frequency semicircle is related to the lithium ion migration through the interface between the surface layer of the particles and the electrolyte, the resistance of Rct. The low-frequency oblique line is attributed to the diffusion process of lithium ions in the bulk of the electrode material, the Warburg resistance of W. The Nyquist plots are fitted by using the equivalent circuit (as shown in Fig. 7B). During cycling, resistance of Re occurred in liquid electrolyte, shows increased values, such as 2.43 to 7.33 ohms in CH-NCM from the fresh state to 100th cycle. It might be due to the minor cathode material dissolved into electrolyte and/or the minor decomposition of electrolyte.¹² The values of Rct for the CH-NCM cathodes gradually increase from 91.5 ohms when in a fresh state to 351.8 ohms after 100 charge–discharge cycles. The slow increase in Rct upon cycling indicates a relatively stable interface between the CH-NCM electrode and electrolyte and therefore good cycle performance of the CH-NCM cathode.

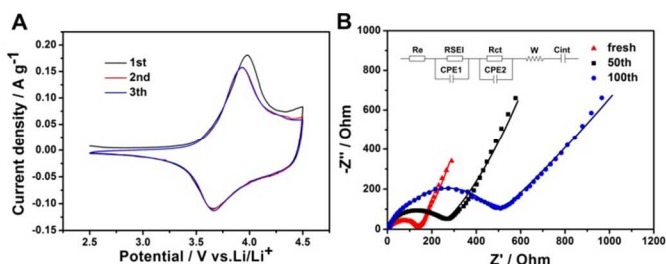


Fig. 7 (A) The cyclic voltammetry (CV) curves of the CH-NCM cathodes in the voltage range of 2.5–4.5 V at the scan rate of 0.1 mV s^{-1} ; (B) Nyquist plots after different charge–discharge cycles for the CH-NCM cathodes. The symbols are the experimental data, whereas the continuous lines are the fitted data.

Conclusion

In summary, we report a simple, fast, and surfactant-free coprecipitation method to synthesize MnCO_3 cubes for the first time, coupled with heat treatment, to prepare ternary cathode cube-shaped hierarchical $\text{LiNi}_{1/3}\text{Co}_{1/3}\text{Mn}_{1/3}\text{O}_2$ (CH-NCM) with enhanced growth of crystal planes in favor of Li^+ intercalation/deintercalation. The special structure endows the material with ultrafast Li^+

intercalation/deintercalation and good structural stability, yielding superior electrochemical performances, especially in terms of rate capability. Therefore, CH-NCM would be a promising cathode to be applied in high performance lithium-ion batteries, which could play an important role in vehicle applications.

Acknowledgements

This work was financially supported by the National Natural Science Foundation of China (Grant No. 50972017 and 21371023) and Research Fund for the Doctoral Program of Higher Education of China (Grant No.20101101110026).

Notes and references

^a Research Center of Materials Science, Beijing Institute of Technology, Beijing 100081, China. Fax: +86 10 68912001; Tel: +86 10 68913792; E-mail: cbcao@bit.edu.cn.

^b Department of Material Science and Engineering, Luoyang Institute of Science and Technology, Luoyang 471023, China

- P. Gibot, M. Casas-Cabanas, L. Laffont, S. Levasseur, P. Carlach, S. Hamelet, J. M. Tarascon and C. Masquelier, *Nat. Mater.*, 2008, 7, 741.
- J. M. Tarascon and M. Armand. *Nature*, 2001, 414, 359.
- Y. K. Sun, D. H. Kim, C. S. Yoon, S. T. Myung, J. Prakash and K. Amine, *Adv. Funct. Mater.*, 2010, 20, 485.
- M. Oljaca, B. Blizanac, A. D. Pasquier, Y. Sun, R. Bontchev, A. Suszko, R. Wall and K. Koehlert, *J. Power Sources*, 2014, 248, 729.
- J. Li, C. Cao, X. Xu, Y. Zhu and R. Yao, *J. Mater. Chem. A*, 2013, 1, 11848.
- Z. Yang, J. Lu, D. Bian, W. Zhang, X. Yang, J. Xia, G. Chen, H. Gu and G. Ma, *J. Power Sources*, 2014, 272, 144.
- L. Wu, K. W. Nam, X. Wang, Y. Zhou, J. C. Zheng, X. Q. Yang and Y. Zhu, *Chem. Mater.*, 2011, 23, 3953.
- F. Fu, G. L. Xu, Q. Wang, Y. P. Deng, X. Li, J. T. Li, L. Huang and S. G. Sun, *J. Mater. Chem. A*, 2013, 12, 3860.
- J. Li, S. Xiong, Y. Liu, Z. Ju and Y. Qian, *Nano Energy*, 2013, 2, 1249.
- W. H. Ryu, S. J. Lim, W. K. Kim and H. Kwon, *J. Power Sources*, 2014, 257, 186.
- J. Li, R. Yao and C. Cao, *ACS Appl. Mater. Interfaces*, 2014, 6, 5075.
- P. Gao, Y. H. Li, H. D. Liu, J. Pinto, X. F. Jiang and G. Yanga, *J. Electrochem. Soc.*, 2012, 159, A506.
- W. B. Hua, X. D. Guo, Z. Zheng, Y. J. Wang, B. H. Zhong, B. Fang, J. Z. Wang, S. L. Chou and H. Liu, *J. Power Sources*, 2015, 275, 200.
- W. Xiong, Y. Jiang, Z. Yang, D. Li and Y. Huang, *J. Alloys Compd.*, 2014, 589, 615.
- J. H. Park, J. H. Cho, S. B. Kim, W. S. Kim, S. Y. Lee and S. Y. Lee, *J. Mater. Chem.*, 2012, 22, 12574.
- C. T. Hsieh, C. Y. Mo, Y. F. Chen and Y. J. Chung, *Electrochim. Acta*, 2013, 106, 525.
- J. X. Zhu, T. Vo, D. S. Li, R. Lu, N. Kinsinger, L. Xiong, Y. S. Yan and D. Kisailus, *Cryst. Growth Des.*, 2012, 12, 1118.
- J. Dou, X. Kang, T. Wumaier, H. Yu, N. Hua, Y. Han and G. Xu, *J. Solid State Electrochem.*, 2012, 16, 1481.
- K. M. Shaju and P. G. Bruce, *Adv. Mater.*, 2006, 18, 2330.
- L. Zhou, D. Zhao and X. W. Lou, *Angew. Chem., Int. Ed.*, 2012, 51, 239.

ARTICLE

21. L. Yang, S. Wang, J. Mao, J. Deng, Q. Gao, Y. Tang and O. G. Schmidt, *Adv. Mater.*, 2013, 25, 1180.
22. J. Hou, C. Cao, F. Idrees and X. Ma, *ACS Nano*, 2015, 9, 2556.
23. L. Chen, Y. Su, S. Chen, N. Li, L. Bao, W. Li, Z. Wang, M. Wang and F. Wu, *Adv. Mater.*, 2014, 26, 6756.
24. J. Xiao, L. Wan, S. Yang, F. Xiao and S. Wang, *Nano Lett.*, 2014, 14, 831.
25. D. Wang, I. Belharouak, G. Zhou and K. Amine, *Adv. Funct. Mater.*, 2013, 23, 1070.
26. L. Zhang, N. Li, B. Wu, H. Xu, L. Wang, X. Q. Yang and F. Wu, *Nano Lett.*, 2015, 15, 656.
27. L. Zhou, D. Zhao and X. W. Lou, *Adv. Mater.*, 2012, 24, 745.
28. H. B. Lin, J. N. Hu, H. B. Rong, Y. M. Zhang, S. W. Mai, L. D. Xing, M. Q. Xu, X. P. Li and W. S. Li, *J. Mater. Chem. A*, 2014, 24, 9272.
29. H. B. Lin, Y. M. Zhang, H. B. Rong, S. W. Mai, J. N. Hu, Y. H. Liao, L. D. Xing, M. Q. Xu, X. P. Li and W. S. Li, *J. Mater. Chem. A*, 2014, 30, 11987.
30. M. J. Aragón, B. León, C. P. Vicent and J. L. Tirado, *J. Power Sources*, 2011, 196, 2863.
31. J. Bai, X. Li, G. Liu, Y. Qian and S. Xiong, *Adv. Funct. Mater.*, 2014, 24, 3012.
32. J. B. Fei, Y. Cui, X. H. Yan, W. Qi, Y. Yang, K. W. Wang, Q. He and J. B. Li, *Adv. Mater.*, 2008, 20, 452.
33. Z. D. Huang, X. M. Liu, S. W. Oh, B. Zhang, P. C. Ma and J. K. Kim, *J. Mater. Chem.*, 2011, 21, 10777.
34. Y. Cho, S. Lee, Y. Lee, T. Hong and J. Cho, *Adv. Energy Mater.*, 2011, 1, 821.
35. C. Nithya, V. S. Syamala Kumari and S. Gopukumar, *Phys. Chem. Chem. Phys.*, 2011, 13, 6125.
36. K. M. Shaju, G. V. Subba Rao, B. V. R. Chowdari, *Electrochim. Acta*, 2002, 48, 145.
37. F. Wu, G. Tan, J. Lu, R. Chen, L. Li and K. Amine, *Nano Lett.*, 2014, 14, 1281.
38. G. M. Koenig, I. Belharouak, H. M. Wu and K. Amine, *Electrochim. Acta*, 2011, 56, 1426.

Table of contents entry

Hierarchical cubed $\text{LiNi}_{1/3}\text{Co}_{1/3}\text{Mn}_{1/3}\text{O}_2$ cathodes with enhanced growth of electrochemical active planes exhibit enhanced electrochemical performances.

